EMN: Brain-inspired Elastic Memory Network for Quick Domain Adaptive Feature Mapping

Jianming Lv [1] **Chengjun Wang** [1] **Depin Liang** [1] **Qianli Ma** [1] **Wei Chen** [2] **Xueqi Cheng** [2]

Abstract

Utilizing unlabeled data in the target domain to perform continuous optimization is critical to enhance the generalization ability of neural networks. Most domain adaptation methods focus on time-consuming optimization of deep feature extractors, which limits the deployment on lightweight edge devices. Inspired by the memory mechanism and powerful generalization ability of biological neural networks in human brains, we propose a novel gradient-free Elastic Memory Network, namely EMN, to support quick fine-tuning of the mapping between features and prediction without heavy optimization of deep features. In particular, EMN adopts randomly connected neurons to memorize the association of features and labels, where the signals in the network are propagated as impulses, and the prediction is made by associating the memories stored on neurons based on their confidence. More importantly, EMN supports reinforced memorization of feature mapping based on unlabeled data to quickly adapt to a new domain. Experiments based on four cross-domain real-world datasets show that EMN can achieve up to 10% enhancement of performance while only needing less than 1% timing cost of traditional domain adaptation methods.

1. Introduction

Most deep ANNs depend on a large scale of labeled data to achieve superior performance and tend to overfit the training sets while optimizing a deep network with a large number of parameters. Especially in the visual classification tasks, directly transferring a deep model across different domains usually yields a significant drop in performance (Donahue et al., 2014).

[1]South China University of Technology, Guangzhou, Guangdong, China [2]Chinese Academy of Sciences, Beijing, China. Correspondence to: Jianming Lv <jmlv@scut.edu.cn>.

Recently, some Unsupervised Domain Adaptation (UDA) methods have been proposed to utilize the unlabeled data in the target domain to continuously optimize the model. In particular, the pseudo-label based methods (Liang et al., 2020; 2021; Litrico et al., 2023) assign the data in the target domain with pseudo labels to optimize the model in a supervised mode. The clustering based methods (Liang et al., 2020; Li et al., 2021) utilize the relationship between the unlabeled samples to fine-tune the deep model. Meanwhile, as a popular technique, the adversarial learning methods (Ganin & Lempitsky, 2015; Zhang et al., 2018; Yang et al., 2022) are usually used to reduce the cross-domain diversity of feature distributions.

The manipulation of pseudo labels and optimization of the deep features in the above UDA methods are usually much more time-consuming compared with the inference procedure, which increases the difficulty of supporting continuous learning on lightweight edge devices. Is it possible to freeze the feature extractor and only fine-tune the mapping between the features and predictions to efficiently enhance the performance on the unlabeled target domain? This is an interesting and practical problem, which is defined as the **Domain Adaptive Feature Mapping (DAMap)** problem in this paper.

Compared with ANNs, the biological neural networks (BNN) in human brains work much better in this aspect, which can adapt to the new domain quickly and update the network efficiently with no need for large amounts of labeled data. Meanwhile, as pointed out by Hinton (Hinton, 2022), there is no direct proof of explicit gradient back-propagation procedure in BNN. Different from the gradient-based function fitting in ANN, BNN seems to take a totally different manner to memorizing the association between signals. The research (Pi et al., 2008) pointed out that memory in brains plays an important role in pattern recognition, which contains three typical stages in the learning and memory process: encoding, storage, and retrieval (Melton, 1963). Some recent research (Roy et al., 2022) showed that the neural cells in brains involved in memory are distributed throughout the entire brain, achieving distributed memory through complex interconnection, rather than being limited to the traditional hippocampus or cerebral cortex.

Inspired by the memory mechanism of brains, we try another way to propose a novel gradient-free Elastic Memory Network, namely EMN, to support quick *Domain Adaptive Feature Mapping*, which mimics the behavior of brains in the following aspects. 1) Neurons are connected randomly and signals are transmitted in the form of impulses without continuous activation inspired by the spiking activities in brains (Maass, 1997). 2) Without using the gradient back-propagation, only forwarding is required to process the impulse signal, which is accumulated in the memory units on each neuron and recorded in fuzzy Gaussian distributions to form the memory storage. 3) The distributed memories are retrieved and integrated based on the confidence to make the final decision of classification; 4) Reinforced memorization of the unlabeled data is supported to adapt the model to the target domain efficiently.

Comprehensive experiments based on four cross-domain real-world datasets show that EMN can efficiently improve the association between input features and labels in the unlabeled target domain. In particular, EMN can achieve up to 10% enhancement of performance while only needing less than 1% timing cost of traditional domain adaptation methods.

The main contributions of this paper are summarized as follows:

- We present a novel brain-inspired gradient-free Elastic Memory Network, namely EMN, for efficient domain adaptive feature mapping, which models the classification tasks as the distributed memory storage and retrieval procedure on randomly connected neurons.
- We propose an impulse based information transmission mechanism by introducing the accumulation behavior in neurons, so as to achieve the non-linear transformation of signals. We further utilize multiple Gaussian distributions to simplify the memory storage and adopt the fuzzy memory based on Gaussian blur to reduce the over-fitting problem.
- We design a reinforced memorization mechanism of EMN, which supports lightweight and efficient optimization of feature mapping based on unlabeled data in the target domain.

2. Related works

2.1. Unsupervised Domain Adaptation (UDA)

Unsupervised Domain Adaptation (UDA) methods have been extensively investigated for various application scenarios, including object recognition (Gopalan et al., 2013; Csurka, 2017; Long et al., 2018) and semantic segmentation (Hoffman et al., 2018; Zou et al., 2018; Zhang et al., 2019; Toldo et al., 2020). UDA methods (Pan & Yang, 2009; Candela et al., 2009) focus on training a learner across domains, which is usually achieved by aligning the diverse cross-domain distributions or learning pseudo labels on the target domain.

In particular, Wang et al. (Wang et al., 2023) achieved domain alignment by minimizing the distance between cross-domain samples. Xie et al. (Xie et al., 2022) proposed a collaborative alignment framework to learn domain-invariant representations by utilizing adversarial training or minimizing the Wasserstein distance between two distributions. Hu et al. (Hu & Lee, 2022) introduced a novel distance-of-distance loss that can effectively measure and minimize domain differences without any external supervision. Du et al. (Du et al., 2021) proposed a method of cross-domain gradient difference minimization, which explicitly minimizes the gradient differences generated by the source and target samples.

The adversarial learning is another commonly used technique to minimize the difference in cross-domain features. In particular, Yang et al. (Yang et al., 2022) proposed a dual-module network architecture that incorporates a domain recognition feature module. This architecture undergoes adversarial training by maximizing the loss of feature distribution and minimizing the discrepancy in prediction results. The Collaborative Adversarial Network (CAN) (Zhang et al., 2018) made the feature extractor and classifier cooperate in shallow layers while competing in deep layers to generate specific yet cross-domain features. In order to utilize the discriminative information in classifier labels, the Conditional Adversarial domain adaptation(CDAN) (Long et al., 2018) attempted to align deep features based on classifier labels.

Recently, learning the pseudo labels predicted by the classifiers on the target domain has been proven quite useful for domain adaptation. In particular, SHOT (Liang et al., 2020) adopted self-supervised pseudo-labeling to implicitly align representations from the target domains to the source hypothesis. Litrico M et al.(Litrico et al., 2023) introduced a novel loss re-weighting strategy, assessing the reliability of refined pseudo-labels via estimating their uncertainty. Liang et al. (Liang et al., 2021) proposed a pseudo-labeling framework aimed at reducing classification errors by introducing an auxiliary classifier solely for the target data, thereby enhancing the quality of the pseudo-labels. Li et al.(Li et al., 2021) proposed a cross-domain adaptive clustering method, which introduces an adversarial adaptive clustering loss to facilitate both inter-domain and intra-domain adaptation.

All of the above methods require time-consuming optimization of deep features based on gradient back-propagation and are only suitable to be run on the server side.

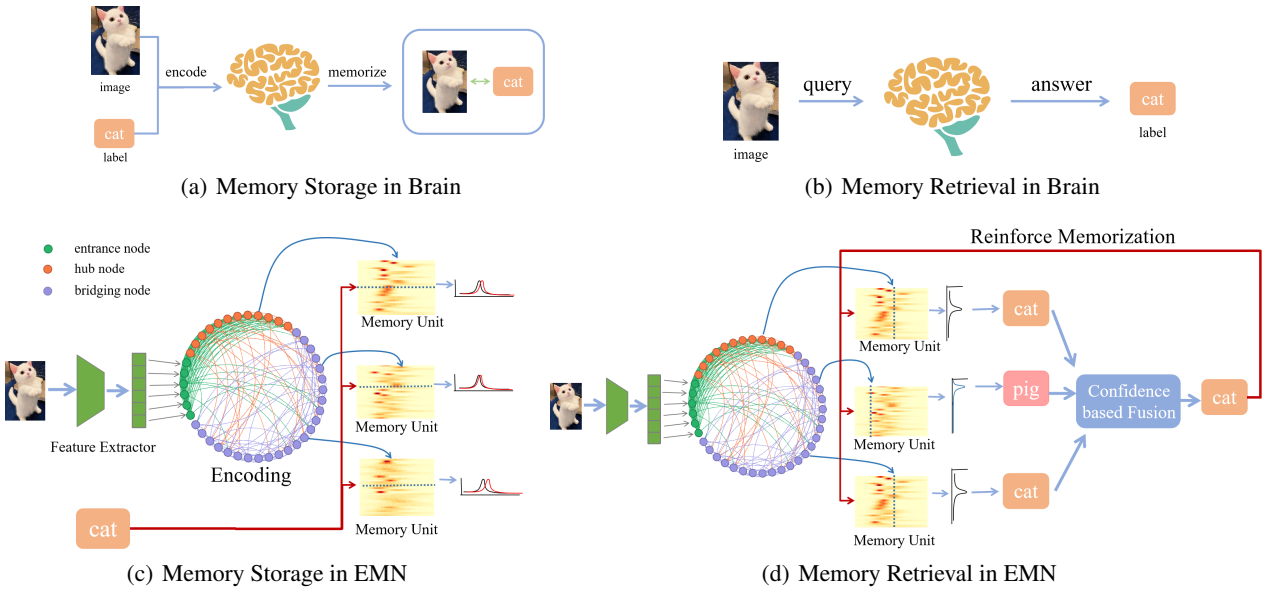

Figure 1. The framework of EMN including the memory storage and the memory retrieval stages compared with brains.

2.2. ANNs without Gradient Back-propagation

Besides the gradient back-propagation based neural networks, there are also some gradient-free network structures, such as the Extreme Learning Machine (ELM) and some of their variants (Cambria et al., 2013; Huang, 2015; Tang et al., 2015). ELM adopted the randomized initialized network for the random projection of features and fitted the linear function on these non-linear features. Following a similar idea to ELM, the Broad Learning System (BLS) (Chen & Liu, 2017) extended the network to support incremental learning for newly added dynamic features. The Echo State Network (ESN) (Jaeger, 2002) adopted a random projection network to achieve the non-linear features of time series. The Liquid State Machine (LSM) (Maass et al., 2002) represents a distinct variant of spiking neural networks, characterized by randomly interconnected nodes that concurrently receive inputs from external sources and other nodes within the network. The recently proposed Forward-Forward algorithm (Hinton, 2022) attempted to use two forward processes with positive and negative data respectively to replace the forward and backward processes in the back-propagation algorithms.

The fundamental difference between EMN and above methods. All of the above methods are designed to fit a function mapping the input to the output, while EMN memorizes the association between input and output on distributed neurons and is able to perform reinforced memorization on the unlabeled target domain.

3. METHODOLOGY

3.1. Problem Definition of DAMap

Most of the visual classification model can be formulated as the function $c(f(x))$, where f is the feature extractor based on the deep models such as ResNet (He et al., 2016) and c is the light-weight classifier such as MLP (Rosenblatt, 1958; Rumelhart et al., 1986) to map the features to output. Given a labeled source domain $D_s = (x_i^s, y_i^s)_{i=1}^{n_s}$ and unlabeled target domain $D_t = (x_i^t)_{i=1}^{n_t}$, the **Domain Adaptive Feature Mapping (DAMap)** aims to transfer the model trained on D_s to D_t, and utilize the unlabeled data in D_t to optimize c while freezing the deep feature extractor f. DAMap avoids the time-consuming optimization of deep feature extractors and is suitable for the lightweight fine-tuning of visual models on edge devices.

3.2. Overview of Elastic Memory Network

As shown in Fig. 1, inspired by the memory storage and retrieval stages of human brains, the Elastic Memory Network (EMN) contains four basic memory-based key procedures: 1) **Memory Encoding** via impulse-based transmission in randomly connected neural networks achieves non-linear projection of the input features; 2) **Distributed Memory Storage** simplified as multiple Gaussian distributions records the association between the features and the labels; 3) **Memory Retrieval** aims to make predictions by integrating the decision on distributed memory units according to memory confidence; 4) **Reinforced Memorization** continuously fine-tunes the memories for domain adaptation according to the predicted labels. The pipeline of EMN will

be detailed in the following sections.

3.3. Memory Encoding via Random Projection

Inspired by the analysis of the brain network structure (Bassett & Sporns, 2017), which contains highly connected hub nodes as well as sparse linked ones, we adopt a hybrid network topology in EMN including three types of nodes: entrance nodes, hub nodes, and bridging nodes. As shown in Fig. 1, the entrance nodes accept the input features and are densely connected to the hub nodes. The bridging nodes are randomly and sparsely connected by all of the other nodes. The edges are all directed and the weights on all edges are randomly initialized in the range $[-1, 1]$.

After the features are fed to the entrance nodes, the signals are propagated in the network through the edges in multiple rounds. Each node accumulates the incoming signals and is activated intermittently to form the impulse-like output to mimic the spiking activity in brains:

$$h_{i,t+1} = h_{i,t} + \sum_{j \in \mathbb{N}_i} o_{j,t} W_{ji} \tag{1}$$

$$o_{i,t+1} = \begin{cases} h_{i,t+1} & if(h_{i,t+1} > 0) \\ 0 & else \end{cases} \tag{2}$$

$$h_{i,t+1} = \begin{cases} 0 & if(h_{i,t+1} > 0) \\ h_{i,t+1} & else \end{cases} \tag{3}$$

$$m_{i,t+1} = m_{i,t} + o_{i,t+1} \tag{4}$$

$$\hat{m}_i = m_{i,T} \tag{5}$$

Here $h_{i,t}$ and $o_{i,t}(0 \le i < N)$ indicate the hidden state and output value individually of the i^{th} node in EMN. In the $t^{th}(0 \le t \le T)$ round of propagation, the signals collected from the predecessor neighbors are accumulated in the hidden state on each node as shown in Eq (1), where the node j is the predecessor neighbor of the node i, and W_{ji} is the weight of the edge from j to i. While the hidden state of a node is larger than the threshold 0, the neuron is activated with the value of the hidden state as Eq (2). Otherwise, the output is 0 in this round. Once the neuron is activated, the hidden state is cleared as Eq (3). The output signal is accumulated as the memory signal $m_{i,t}$ as Eq (4), which will be recorded in the memory storage in the future. When an input feature vector $X = (x_1, x_2, ..., x_n)$ is fed to the entrance nodes, the output signal $o_{i,0}(1 \le i \le n)$ of the entrance nodes is initialized as x_i, while $o_{i,0}$ of other nodes are all initialized as zero. Meanwhile, $m_{i,0}$ and $h_{i,0}$ are all set as zero at the beginning. The steady memory signal of the node i is defined as $\hat{m}_i$ in Eq (5), where T is the max number of the rounds.

3.4. Distributed Memory Storage

Inspired by the distributed memory in brains, each node of EMN maintains the memory about the association between the accepted memory signal $\hat{m}$ and the label y for each input instance as shown in Fig. 1(c). The memory unit of the i^{th} neuron node can be modeled as a two-dimensional image M_i, the first dimension of which is the class label y and the other one is the memory signal $\hat{m}$. For each incoming feature vector, which is propagated in the network to achieve the memory signal on each neuron by Eq (5), the association of the memory signal and the label of the instance can be stored by increasing the value of the corresponding pixel in M_i. However, this trivial implementation of memory storage may lead to a large consumption of computer memory.

To reduce the memory cost, we adopt multiple Gaussian distributions to approximate the memory storage. In particular, for the visual classification tasks, we assume that the distribution of memory signals in the k^{th} class on the i^{th} neuron obeys the Gaussian distribution:

$$Pr(\hat{m}_i | y = k) = \frac{1}{\sqrt{2\pi\sigma_i^k}} exp(-\frac{(\hat{m}_i - \mu_i^k)^2}{2\sigma_i^k}) \tag{6}$$

In this way, the storage of memory unit M_i can be represented as C Gaussian distribution $\{N(\mu_i^k, \sigma_i^k) | 1 \le k \le C\}$ with $2 * C$ learnable parameters, where C is the number of classes.

While training EMN on the labeled source domain, the parameters are incrementally updated in batch as follows:

$$\mu_i^k = \beta\mu_i^k + (1 - \beta)\frac{1}{B}\sum_{b=1}^{B} \hat{m}_{i,b}^k \tag{7}$$

$$\sigma_{i,b}^k = \beta\sigma_{i,b}^k + (1 - \beta)\frac{1}{B}\sum_{b=1}^{B} \sqrt{(\hat{m}_{i,b}^k - \mu_i^k)^2} \tag{8}$$

β denotes the temperature parameter between batches and B denotes the batch size. $\hat{m}_{i,b}^k$ denotes the memory signal received on the i^{th} node while processing the b^{th} instance belonging to the k^{th} class.

Meanwhile, the above memory based learning relies on fitting the probability distribution, so a smaller size of the training set or imbalanced label distribution may cause the over-fitting of the distribution function on insufficient samples. To increase the generalization ability of the model, we introduce the Gaussian blur on the memorized Gaussian distribution (Eq (6)) with the Gaussian kernel function

$g(x_1, x_2) = exp(-\frac{(x_1-x_2)^2}{2\sigma_1})$ to achieve the fuzzy memory:

$$\begin{aligned} Q(\hat{m}_i|y=k) &= \int_{-\infty}^{+\infty} Pr(\hat{m}|y=k)g(\hat{m},\hat{m}_i)d\hat{m} \\ &= \frac{\sqrt{\sigma_1}}{2\sqrt{2\sigma_i^k+\sigma_1}} exp(-\frac{(\hat{m}_i-\mu_i^k)^2}{2\sigma_i^k+\sigma_1}) \end{aligned} \tag{9}$$

3.5. Confidence based Memory Retrieval

The pipeline of memory retrieval on EMN is shown in Fig. 1(d). After the input features of an instance are fed to the entrance nodes and propagated in the network, the i^{th} node will receive the memory signal $\hat{m}_i$ as Eq (5) and retrieve its memory unit to gain the conditional probability inference as follows:

$$Pr(y=k|\hat{m}_i) = \frac{Q(\hat{m}_i|y=k)}{\sum_{c=1}^{C} Q(\hat{m}_i|y=c)} \tag{10}$$

Here $Q(\hat{m}_i|y=k)$ indicates the fuzzy memory distribution (Eq (9)) achieved at the memory storage stage. The most likely class label predicted by the i^{th} node is

$$K_i = \arg\max_k Pr(y=k|\hat{m}_i) \tag{11}$$

The confidence of the node to make the prediction can be defined as the likelihood of the memory signal as follows:

$$c_i = Q(\hat{m}_i|y=K_i) \tag{12}$$

The final decision of the whole network is defined as the confidence-based fusion of the predictions of all neurons:

$$Pr(y=k|X) = \frac{c_i Pr(y=k|\hat{m}_i)}{\sum_j^N c_j} \tag{13}$$

The predicted label is as follows:

$$\hat{y} = \arg\max_k Pr(y=k|X) \tag{14}$$

3.6. Reinforced Memorization for Domain Adaptation

The pairs of samples and pseudo labels $\{(X, \hat{y})\}$ can be fed to EMN to conduct reinforced memorizing of the association between the features and labels by updating the parameters according to Eq (7) and (8).

As reported by (Litrico et al., 2023), the noise of pseudo labels affects the performance of UDA significantly, which may bring the accumulation of errors and make the model over-fit the wrong prediction. To reduce the oscillation of the model caused by the noise, we introduce the confidence E_i of parameter updating on the node i by measuring the likelihood that the node makes the same prediction as the pseudo label $\hat{y}$:

$$E_i(\hat{m}_i, \hat{y}) = Q(\hat{m}_i|y=\hat{y}) \tag{15}$$

Then the updating of parameters in Eq (7) and (8) is rewritten as follows:

$$\mu_i^{\hat{y}} = \beta\mu^{\hat{y}} + (1-\beta)\frac{1}{B}\sum_{b=1}^{B} E_i(\hat{m}_{i,b}^{\hat{y}}, \hat{y})\hat{m}_{i,b}^{\hat{y}} \tag{16}$$

$$\sigma_{i,b}^{\hat{y}} = \beta\sigma_{i,b}^{\hat{y}} + (1-\beta)\frac{1}{B}\sum_{b=1}^{B} E_i(\hat{m}_{i,b}^{\hat{y}}, \hat{y})\sqrt{(\hat{m}_{i,b}^{\hat{y}} - \mu_i^{\hat{y}})^2} \tag{17}$$

The pseudo label with higher confidence on a neuron node will achieve higher weight to update the parameters on the node. After updating the parameters, the model can generate new pseudo labels on the unlabeled data. In this way, the updating can be run in multiple iterations to reinforce the memorization in a self-supervised way, so as to make the learned distribution approach the ground-truth target distribution, which is based on the supervised learning on the target domain, as shown in Fig. 4.

4. Experiments

4.1. Experimental Setup

Datasets. Comprehensive experiments for DAMap are conducted on the following four popularly used cross-domain datasets:

- Digits: The classic digit image datasets from 3 different domains: MNIST (LeCun et al., 1998) (M), USPS (Hull, 1994) (U), and SVHN (Netzer et al., 2011) (S). Following the evaluation protocol of CyCADA (Hoffman et al., 2018), three cross-domain transfer tasks are evaluated : USPS to MNIST (U $\rightarrow$ M), MNIST to USPS (M $\rightarrow$ U), and SVHN to MNIST (S $\rightarrow$ M).

- Office-31: Office-31 Dataset (Saenko et al., 2010) is the most widely used dataset for visual domain adaptation, consisting of 4,110 images from 31 categories collected from three different domains: Amazon (A), Webcam (W) and DSLR (D). All possible combinations of the domains are tested as the transfer tasks.

- Office-Home: Office-Home dataset (Venkateswara et al., 2017) is a challenging medium-sized benchmark with four distinct domains containing 65 categories: Artistic images (A), Clip Art (C), Product images (P), and Real-World images (R). All possible combinations of the domains are tested as the transfer tasks.

- VisDA-C: VisDA-C (Peng et al., 2017)is a challenging large-scale benchmark that mainly focuses on the 12-class object recognition task containing two domains: the Synthesis(S) which contains 152 thousand synthetic images generated by rendering 3D models, and

Table 1. Accuracy(%) of DAMap methods on VisDA-C.

Method	$S \rightarrow R$	$R \rightarrow S$	Avg.
w/o DA	54.83	65.06	59.95
BLS	59.43	75.05	<u>67.24</u>
KNN	58.60	66.70	62.65
DCT	32.50	47.59	40.05
RFS	49.30	66.22	57.76
MLP	57.84	72.13	64.99
SVM	53.60	68.64	61.12
BAG	59.02	67.43	63.23
NBY	46.75	78.19	62.47
XGBoost	47.62	66.27	56.95
EMN(OURS)	**62.47**	**81.68**	**72.08**

Table 2. Accuracy(%) of DAMap methods on Digits

Method	$S \rightarrow M$	$M \rightarrow U$	$U \rightarrow M$	Avg.
w/o DA	72.36	79.16	87.27	79.60
BLS	80.80	92.45	**93.88**	<u>89.04</u>
KNN	77.62	92.07	91.70	87.13
DCT	56.04	77.43	66.24	66.57
RFS	73.83	91.19	88.54	84.52
MLP	77.14	91.57	92.06	86.92
SVM	75.45	92.57	91.64	86.55
BAG	78.36	**92.68**	92.46	87.83
NBY	81.12	91.75	89.53	87.47
XGBoost	73.07	89.78	87.39	83.42
EMN(OURS)	**82.45**	91.18	93.79	**89.14**

the Real(R) which has 55 thousand real object images sampled from Microsoft COCO. All possible combinations of the domains are tested as the transfer tasks: S $\rightarrow$ R, and R $\rightarrow$ S.

Evaluation Metrics. Following the definition of the DAMap challenge, we train the model on the labeled source domain and optimize it based on the unlabeled data in the target domain while freezing the feature extractor. The accuracy of classification and timing cost is evaluated in the target domain.

Baselines of DAMap. EMN is compared with the following DAMap baselines, which are commonly used classifiers to map features to labels.

- MLP (Rosenblatt, 1958; Rumelhart et al., 1986). The Multi-layer Perceptron with a hidden layer having 3096 units and a ReLU activation.
- BLS (Chen & Liu, 2017). The Broad Learning System with 500 enhancement nodes is used and performs 5 incremental steps.
- SVM (Cortes & Vapnik, 1995). The Radial Basis Function (RBF) kernel is used with the gamma parameter set to 'auto' in `sklearn`.
- KNN (Cover & Hart, 1967; Altman, 1992). The KNN model 'KNeighborsClassifier' from `sklearn` with 5 neighbors and uniform weights.
- DCT (Quinlan, 1987). The Decision Tree model with the default configuration from `sklearn`.
- XGBoost (Chen & Guestrin, 2016). The number of trees is 100 and the maximum depth of each tree is 6. The learning rate is set to 0.3 to control the step size during the gradient boosting process.
- RFS (Breiman, 2001). The Random Forest model using 'RandomForestClassifier' from `sklearn` with 100 estimators.
- BAG (Breiman, 1996). The Bagging method ensembling 10 KNN base models.
- NBY (Hand & Yu, 2001). The Naive Bayesian algorithm using the default configuration from `sklearn`.

Furthermore, we use 'w/o DA' to indicate transferring the model directly without any further fine-tuning on the target domain.

Baselines of UDA. We also compare EMN with the following typical UDA methods.

- DANN (Ganin & Lempitsky, 2015) is a classical adversarial UDA method based on the Gradient Reverse Layer.
- CDAN (Long et al., 2018) is a conditional adversarial UDA method which utilizes the discriminative information in classifier labels to align deep features accross different domains.
- SHOT (Liang et al., 2020) adopts self-supervised pseudo-labeling to implicitly align representations from the target domains to the source hypothesis.
- TPDS (Tang et al., 2024) propose a target prediction distribution searching paradigm to overcome the domian shift.

Network Configurations of DAMap. Under the setting of Domain Adaptive Feature Mapping (DAMap), the feature extractor is frozen while only fine-tuning the mapping between features and output labels. For a fair comparison, EMN and all baselines of DAMap use the same frozen features coming from the same feature extractors.

In particular, we utilize the LeNet-5(LeCun et al., 1998) as the feature extractors for the simple digital recognition task in the Digits dataset. For the object recognition tasks, we adopt the pre-trained ResNet (He et al., 2016) models as feature extractors (ResNet-101 for VisDA-C, and ResNet-50 for Office-31 and Office-Home), following the experimental

Table 3. Accuracy(%) of DAMap methods on Office-31

Method	$A \rightarrow D$	$D \rightarrow W$	$W \rightarrow A$	Avg.
w/o DA	80.52	94.72	63.15	79.04
BLS	80.92	94.84	65.99	80.44
KNN	89.96	94.97	62.80	82.34
DCT	41.37	39.87	24.99	36.18
RFS	81.53	89.69	58.71	77.16
MLP	84.34	94.21	64.71	80.44
SVM	83.53	94.72	62.41	79.62
BAG	87.34	95.60	64.11	82.64
NBY	84.34	92.58	65.32	80.76
XGB	70.88	71.95	41.39	61.41
EMN	**92.15**	**97.48**	**70.35**	**86.08**

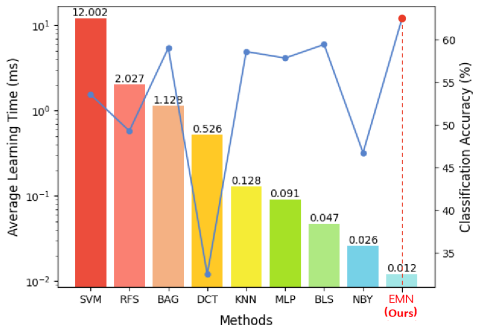

Figure 2. Accuracy versus the average domain adaptation time per instance in different DAMap methods on the $S \rightarrow R$ task of the VisDA-C dataset.

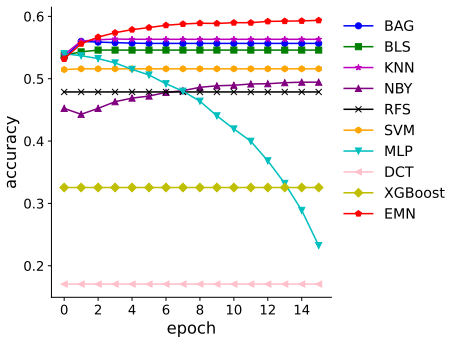

Figure 3. The accuracy in different epochs of domain adaptation on the $P \rightarrow A$ task of the Office-Home dataset.

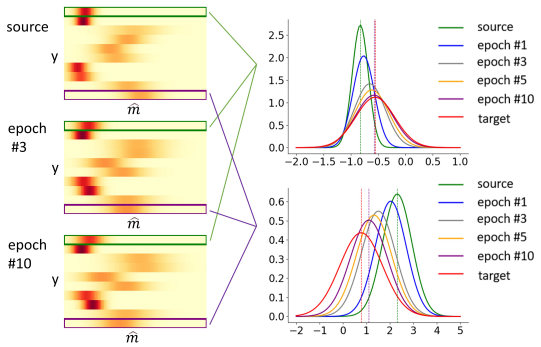

Figure 4. The updating of the memory unit on a neuron while performing the domain adaptation from MNIST to USPS in the Digits dataset.

configurations in previous works like (Deng et al., 2019), (Xu et al., 2019), and (Peng et al., 2019).

While training the feature extractors on the source domains, we adopt mini-batch stochastic gradient descent (SGD) with the momentum as 0.9, weight decay as $1e^{-3}$, and learning rate $\eta = 1e^{-3}$ in VisDA-C and $1e^{-2}$ in other datasets. The batch size is set to 64. All DAMap methods are optimized based on frozen features by running 16 epochs over their self-generated pseudo labels, and the best results are recorded.

In EMN, the number of hub nodes and bridging nodes are both 50, the in-degree of the bridging nodes is 30, and the maximum iterations of propagation T is set as 3 by default.

4.2. Experimental Results

Tables 1, 2, 3, and 4 show the classification accuracy of each DAMap algorithm on the VisDA-C, Digits, Office-31, and Office-Home datasets respectively. It can be observed that EMN has the highest average accuracy across all datasets. Particularly on the S $\rightarrow$ R task on the most challenging dataset VisDA-C with the largest size, EMN increases the accuracy more than 10% compared with the ANN model MLP. Similarly, in the Office-Home and Office-31 datasets, EMN outperforms the other baselines significantly, showcasing its potential as a general classifier in domain adaptation. Fig 2 further illustrates the average time required for self-supervised domain adaptation per sample on the VisDA-C datasets. EMN surpasses all other classifiers significantly, reducing 87% time compared with traditional neural network MLP, which is utilized in most UDA methods as the classifier to map deep features to labels in the last layers of the visual models. EMN is even twice faster than the light-weight NBY model, indicating its good potential for real-time domain adaptation tasks. More results on all datasets are given in the appendix.

We also compare the performance of EMN with typical UDA methods in Table 5. Without heavy fine-tuning of deep features, the time cost of model optimization in EMN is less than 1% of the traditional UDA models, especially in the cases of Office-31 and Office-Home where complex deep backbone networks are deployed. Moreover, even only fine-tuning the feature mapping, EMN can achieve comparable accuracy with the UDA methods.

Fig. 3 further depicts the accuracy of the models over the epochs of learning pseudo labels on the target domain of the Office-Home dataset. More results on all datasets are provided in the appendix. In all cases, EMN can improve the performance steadily, which benefits from the confidence-

Table 4. Accuracy(%) of DAMap methods on Office-Home

Method	$A \to C$	$A \to P$	$A \to R$	$C \to A$	$C \to P$	$C \to R$	$P \to A$	$P \to C$	$P \to R$	$R \to A$	$R \to C$	$R \to P$	Avg.
w/o DA	44.60	68.53	75.07	54.10	63.51	65.60	53.15	40.28	72.48	66.17	46.94	78.55	60.75
BLS	47.03	71.59	75.88	55.34	66.19	67.57	54.59	44.33	74.11	65.84	50.20	78.58	62.60
KNN	44.19	67.11	71.63	54.38	64.72	65.64	56.37	45.52	74.59	66.79	52.39	79.21	61.88
DCT	14.39	24.19	30.62	17.26	23.43	26.83	16.89	13.06	31.63	27.28	17.55	39.20	23.53
RFS	40.87	60.04	68.60	48.54	58.75	60.45	47.88	38.95	69.45	63.21	46.85	76.44	56.67
MLP	46.12	66.77	73.24	54.59	64.18	66.26	54.42	43.99	73.79	66.50	50.13	78.85	61.57
SVM	47.15	69.85	74.86	52.32	63.26	64.59	51.59	42.11	72.71	65.18	48.29	77.90	60.82
BAG	45.15	67.65	72.83	52.74	65.58	64.98	56.00	45.29	74.94	66.96	52.00	78.76	61.91
NBY	48.73	72.58	**77.55**	52.58	67.81	67.82	50.47	40.32	72.05	60.85	47.10	76.66	61.21
XGB	36.75	54.56	63.87	36.59	48.73	49.67	32.55	29.23	56.81	50.52	35.78	66.93	46.83
EMN(OURS)	**50.39**	**76.48**	76.91	**59.27**	**71.11**	**69.65**	**59.89**	**47.30**	**76.47**	**69.54**	**53.90**	**81.03**	**66.00**

Table 5. Accuracy and training time per sample in UDA methods.

Method	Digits		Office-31		Office-Home	
	Acc. (%)	Time (ms)	Acc. (%)	Time (ms)	Acc. (%)	Time (ms)
CDAN	93.1	25.12	86.5	287.95	63.8	686.82
SHOT	98.1	2.88	88.6	67.77	71.8	81.14
TPDS	98.4	23.52	90.2	85.12	73.5	120.61
EMN	90.1	**0.37**	85.4	**0.32**	65.5	**0.57**

Table 6. Classification accuracy(%) of the variation models, where *G* indicates the Gaussian blur based fuzzy memory and *C* indicates the confidence based optimization.

Dataset	base	base+G	base+G+C	
Office-31	73.46	85.45	**86.08**	↑12.62
Office-Home	42.54	64.98	**66.00**	↑ 23.46
Digits	60.68	88.94	**89.14**	↑28.46
VisDA-C	35.94	70.97	**72.08**	↑36.14
average	53.16	77.59	**78.33**	↑25.17

based parameter updating in Eq (16) and (17). It can also be observed that MLP faces a significant drop in performance in some cases, which may be caused by the accumulated errors of noisy pseudo labels.

Visualization Results. Fig. 4 depicts how the memory units evolve along with the iterations of domain adaptation, and highlights the changing of the Gaussian distributions consistent with Eq (7) and (8). After multiple rounds of self-supervised learning on pseudo labels, the distributions effectively approach the target distribution, which corresponds to the model supervised trained using the labels on the target domain. This validates the remarkable effectiveness of EMN in DAMap.

Ablation study. The fuzzy memory based on the Gaussian blur in Eq (9) and the confidence based optimization in Eq (16) and (17) play important roles in increasing the robustness of the memory storage and retrieval. Their effectiveness is tested by the ablation studies in Table 6. It can be observed that the Gaussian blur has a great impact on the performance, which confirms the importance of introducing the fuzzy memory to reduce the overfitting of the distribution function. Table 6 also shows that the combination of all components can achieve the best performance.

4.3. Parameter Analysis

In order to investigate the impact of network scale on the performance of domain adaptation, we conducted a sensitivity analysis of the number of hub nodes and bridging nodes by simultaneously increasing the number of both types of nodes as Fig. 5. It can be observed that the performance gradually improves as the network scale increases, and relatively high performance can be achieved when the number reaches 50.

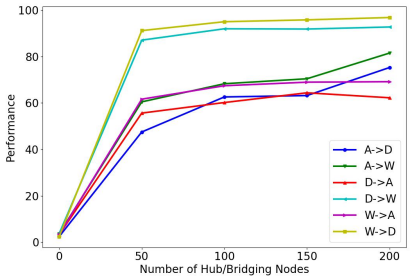

Figure 5. Accuracy versus the number of Hub/Bridging nodes in the Office-31 dataset

Conclusion

In this paper, we propose a novel brain-inspired Elastic Memory Network model, namely EMN, to support efficient Domain-Adaptive Feature Mapping. In particular, EMN learns the association between the features and labels based on the distributed memories on the neurons through impulse-based information transmission and accumulation. EMN is also able to utilize its prediction results on unlabeled data to perform reinforced memorization to support quick domain adaptation. Comprehensive experiments show the superior performance and the low timing cost in EMN, which indicates that EMN has good potential to be run on edge devices for continuous optimization.

In the future, we will further explore the relationship be-

tween the performance and the network topology of EMN inspired by biological neural networks. Meanwhile, we will also extend EMN to support more learning tasks, including the multi-modal DAMap problems, to verify the power of distributed memorization.

Impact Statement

Our research presents a novel brain-inspired neural network to support quick domain adaptation and open a new way of machine learning to model the classification problem as distributed memorization of associations between input signals and labels.

References

Altman, N. S. An introduction to kernel and nearest-neighbor nonparametric regression. *The American Statistician*, 46(3):175–185, 1992.

Bassett, D. S. and Sporns, O. Network neuroscience. *Nature neuroscience*, 20(3):353–364, 2017.

Breiman, L. Bagging predictors. *Machine learning*, 24: 123–140, 1996.

Breiman, L. Random forests. *Machine learning*, 45:5–32, 2001.

Cambria, E., Huang, G.-B., Kasun, L. L. C., Zhou, H., Vong, C. M., Lin, J., Yin, J., Cai, Z., Liu, Q., Li, K., et al. Extreme learning machines [trends & controversies]. *IEEE intelligent systems*, 28(6):30–59, 2013.

Candela, J. Q., Sugiyama, M., Schwaighofer, A., and Lawrence, N. D. Dataset shift in machine learning. *The MIT Press*, 1:5, 2009.

Chen, C. P. and Liu, Z. Broad learning system: An effective and efficient incremental learning system without the need for deep architecture. *IEEE transactions on neural networks and learning systems*, 29(1):10–24, 2017.

Chen, T. and Guestrin, C. Xgboost: A scalable tree boosting system. In *Proceedings of the 22nd acm sigkdd international conference on knowledge discovery and data mining*, pp. 785–794, 2016.

Cortes, C. and Vapnik, V. Support-vector networks. *Machine learning*, 20:273–297, 1995.

Cover, T. and Hart, P. Nearest neighbor pattern classification. *IEEE transactions on information theory*, 13(1):21–27, 1967.

Csurka, G. A comprehensive survey on domain adaptation for visual applications. *Domain adaptation in computer vision applications*, pp. 1–35, 2017.

Deng, Z., Luo, Y., and Zhu, J. Cluster alignment with a teacher for unsupervised domain adaptation. In *Proceedings of the IEEE/CVF international conference on computer vision*, pp. 9944–9953, 2019.

Donahue, J., Jia, Y., Vinyals, O., Hoffman, J., Zhang, N., Tzeng, E., and Darrell, T. Decaf: A deep convolutional activation feature for generic visual recognition. In *International conference on machine learning*, pp. 647–655. PMLR, 2014.

Du, Z., Li, J., Su, H., Zhu, L., and Lu, K. Cross-domain gradient discrepancy minimization for unsupervised domain adaptation. In *Proceedings of the IEEE/CVF conference on computer vision and pattern recognition*, pp. 3937–3946, 2021.

Ganin, Y. and Lempitsky, V. Unsupervised domain adaptation by backpropagation. In *International conference on machine learning*, pp. 1180–1189. PMLR, 2015.

Gopalan, R., Li, R., and Chellappa, R. Unsupervised adaptation across domain shifts by generating intermediate data representations. *IEEE transactions on pattern analysis and machine intelligence*, 36(11):2288–2302, 2013.

Hand, D. J. and Yu, K. Idiot's bayes—not so stupid after all? *International statistical review*, 69(3):385–398, 2001.

He, K., Zhang, X., Ren, S., and Sun, J. Deep residual learning for image recognition. In *Proceedings of the IEEE conference on computer vision and pattern recognition*, pp. 770–778, 2016.

Hinton, G. The forward-forward algorithm: Some preliminary investigations. *arXiv preprint arXiv:2212.13345*, 2022.

Hoffman, J., Tzeng, E., Park, T., Zhu, J.-Y., Isola, P., Saenko, K., Efros, A., and Darrell, T. Cycada: Cycle-consistent adversarial domain adaptation. In *International conference on machine learning*, pp. 1989–1998. Pmlr, 2018.

Hu, C. and Lee, G. H. Feature representation learning for unsupervised cross-domain image retrieval. In *European Conference on Computer Vision*, pp. 529–544. Springer, 2022.

Huang, G.-B. What are extreme learning machines? filling the gap between frank rosenblatt's dream and john von neumann's puzzle. *Cognitive Computation*, 7:263–278, 2015.

Hull, J. J. A database for handwritten text recognition research. *IEEE Transactions on pattern analysis and machine intelligence*, 16(5):550–554, 1994.

Jaeger, H. Adaptive nonlinear system identification with echo state networks. *Advances in neural information processing systems*, 15, 2002.

LeCun, Y., Bottou, L., Bengio, Y., and Haffner, P. Gradient-based learning applied to document recognition. *Proceedings of the IEEE*, 86(11):2278–2324, 1998.

Li, J., Li, G., Shi, Y., and Yu, Y. Cross-domain adaptive clustering for semi-supervised domain adaptation. In *Proceedings of the IEEE/CVF Conference on Computer Vision and Pattern Recognition*, pp. 2505–2514, 2021.

Liang, J., Hu, D., and Feng, J. Do we really need to access the source data? source hypothesis transfer for unsupervised domain adaptation. In *International conference on machine learning*, pp. 6028–6039. PMLR, 2020.

Liang, J., Hu, D., and Feng, J. Domain adaptation with auxiliary target domain-oriented classifier. In *Proceedings of the IEEE/CVF conference on computer vision and pattern recognition*, pp. 16632–16642, 2021.

Litrico, M., Del Bue, A., and Morerio, P. Guiding pseudo-labels with uncertainty estimation for source-free unsupervised domain adaptation. In *Proceedings of the IEEE/CVF Conference on Computer Vision and Pattern Recognition*, pp. 7640–7650, 2023.

Long, M., Cao, Z., Wang, J., and Jordan, M. I. Conditional adversarial domain adaptation. *Advances in neural information processing systems*, 31, 2018.

Maass, W. Networks of spiking neurons: the third generation of neural network models. *Neural networks*, 10(9): 1659–1671, 1997.

Maass, W., Natschläger, T., and Markram, H. Real-time computing without stable states: A new framework for neural computation based on perturbations. *Neural computation*, 14(11):2531–2560, 2002.

Melton, A. W. Implications of short-term memory for a general theory of memory. *Journal of verbal Learning and verbal Behavior*, 2(1):1–21, 1963.

Netzer, Y., Wang, T., Coates, A., Bissacco, A., Wu, B., and Ng, A. Y. Reading digits in natural images with unsupervised feature learning. 2011.

Pan, S. J. and Yang, Q. A survey on transfer learning. *IEEE Transactions on knowledge and data engineering*, 22(10): 1345–1359, 2009.

Peng, X., Usman, B., Kaushik, N., Hoffman, J., Wang, D., and Saenko, K. Visda: The visual domain adaptation challenge. *arXiv preprint arXiv:1710.06924*, 2017.

Peng, X., Bai, Q., Xia, X., Huang, Z., Saenko, K., and Wang, B. Moment matching for multi-source domain adaptation. In *Proceedings of the IEEE/CVF international conference on computer vision*, pp. 1406–1415, 2019.

Pi, Y., Liao, W., Liu, M., and Lu, J. Theory of cognitive pattern recognition. *Pattern recognition techniques, technology and applications*, pp. 626, 2008.

Quinlan, J. R. Generating production rules from decision trees. In *ijcai*, volume 87, pp. 304–307. Citeseer, 1987.

Rosenblatt, F. The perceptron: a probabilistic model for information storage and organization in the brain. *Psychological review*, 65(6):386, 1958.

Roy, D. S., Park, Y.-G., Kim, M. E., Zhang, Y., Ogawa, S. K., DiNapoli, N., Gu, X., Cho, J. H., Choi, H., Kamentsky, L., et al. Brain-wide mapping reveals that engrams for a single memory are distributed across multiple brain regions. *Nature communications*, 13(1):1799, 2022.

Rumelhart, D. E., Hinton, G. E., and Williams, R. J. Learning representations by back-propagating errors. *nature*, 323(6088):533–536, 1986.

Saenko, K., Kulis, B., Fritz, M., and Darrell, T. Adapting visual category models to new domains. In *Computer Vision–ECCV 2010: 11th European Conference on Computer Vision, Heraklion, Crete, Greece, September 5-11, 2010, Proceedings, Part IV 11*, pp. 213–226. Springer, 2010.

Tang, J., Deng, C., and Huang, G.-B. Extreme learning machine for multilayer perceptron. *IEEE transactions on neural networks and learning systems*, 27(4):809–821, 2015.

Tang, S., Chang, A., Zhang, F., Zhu, X., Ye, M., and Zhang, C. Source-free domain adaptation via target prediction distribution searching. *International journal of computer vision*, 132(3):654–672, 2024.

Toldo, M., Maracani, A., Michieli, U., and Zanuttigh, P. Unsupervised domain adaptation in semantic segmentation: a review. *Technologies*, 8(2):35, 2020.

Venkateswara, H., Eusebio, J., Chakraborty, S., and Panchanathan, S. Deep hashing network for unsupervised domain adaptation. In *Proceedings of the IEEE conference on computer vision and pattern recognition*, pp. 5018–5027, 2017.

Wang, Q., Pang, G., Salehi, M., Buntine, W., and Leckie, C. Cross-domain graph anomaly detection via anomaly-aware contrastive alignment. In *Proceedings of the AAAI Conference on Artificial Intelligence*, volume 37, pp. 4676–4684, 2023.

Xie, B., Li, S., Lv, F., Liu, C. H., Wang, G., and Wu, D. A collaborative alignment framework of transferable knowledge extraction for unsupervised domain adaptation. *IEEE Transactions on Knowledge and Data Engineering*, 2022.

Xu, R., Li, G., Yang, J., and Lin, L. Larger norm more transferable: An adaptive feature norm approach for unsupervised domain adaptation. In *Proceedings of the IEEE/CVF international conference on computer vision*, pp. 1426–1435, 2019.

Yang, Y., Zhang, T., Li, G., Kim, T., and Wang, G. An unsupervised domain adaptation model based on dual-module adversarial training. *Neurocomputing*, 475:102–111, 2022.

Zhang, W., Ouyang, W., Li, W., and Xu, D. Collaborative and adversarial network for unsupervised domain adaptation. In *Proceedings of the IEEE conference on computer vision and pattern recognition*, pp. 3801–3809, 2018.

Zhang, Y., David, P., Foroosh, H., and Gong, B. A curriculum domain adaptation approach to the semantic segmentation of urban scenes. *IEEE transactions on pattern analysis and machine intelligence*, 42(8):1823–1841, 2019.

Zou, Y., Yu, Z., Kumar, B., and Wang, J. Unsupervised domain adaptation for semantic segmentation via class-balanced self-training. In *Proceedings of the European conference on computer vision (ECCV)*, pp. 289–305, 2018.

A. More Experimental Results

A.1. Full Results of Classification Accuracy on Office-31

The full table of the classification accuracy on the Office-31 datasets covering all cases of domain transferring is shown in Table 7.

Table 7. Classification accuracy(%) of all tasks on the Office-31 Dataset

	$A \to D$	$A \to W$	$D \to A$	$D \to W$	$W \to A$	$W \to D$	Avg.
DT	80.52	76.73	60.53	94.72	63.15	98.59	79.04
BLS	80.92	79.37	62.12	94.84	65.99	99.40	80.44
KNN	89.96	84.78	61.91	94.97	62.80	**99.60**	82.34
DCT	41.37	35.97	21.44	39.87	24.99	53.41	36.18
RFS	81.53	77.23	56.59	89.69	58.71	99.20	77.16
MLP	84.34	79.75	60.63	94.21	64.71	99.00	80.44
SVM	83.53	77.99	59.89	94.72	62.41	99.20	79.62
BAG	87.34	87.04	62.34	95.60	64.11	99.40	82.64
NBY	84.34	81.64	63.26	92.58	65.32	97.39	80.76
EMN	**92.15**	**88.92**	**68.18**	**97.48**	**70.35**	99.40	**86.08**

A.2. Accuracy versus Timing Cost on all Datasets

The full results about the accuracy and timing cost of different DAMap models are shown in the following Fig. 6, Fig. 7, Fig. 8, and Fig. 9.

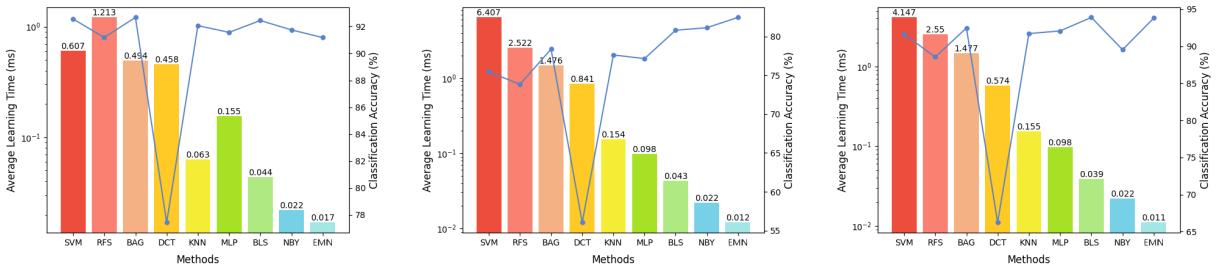

(a) $M \to U$ (b) $S \to M$ (c) $U \to M$

Figure 6. Accuracy versus the average domain adaptation time per instance on the Digits dataset.

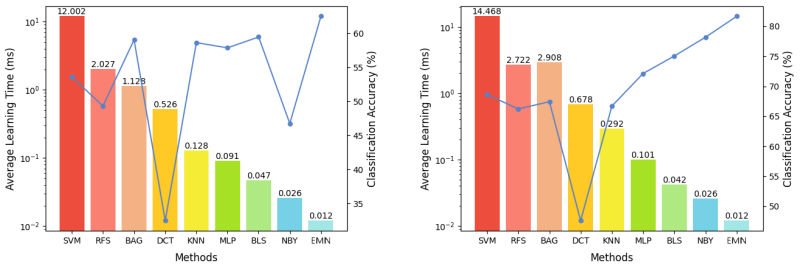

(a) $S \rightarrow R$ (b) $R \rightarrow S$

Figure 7. Accuracy versus the average domain adaptation time per instance on the VisDA-C dataset.

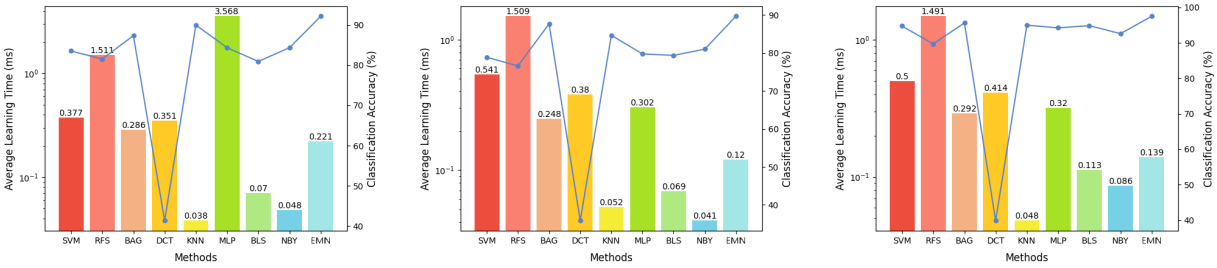

(a) $A \rightarrow D$ (b) $A \rightarrow W$ (c) $D \rightarrow W$

Figure 8. Accuracy versus the average domain adaptation time per instance on the Office-31 dataset.

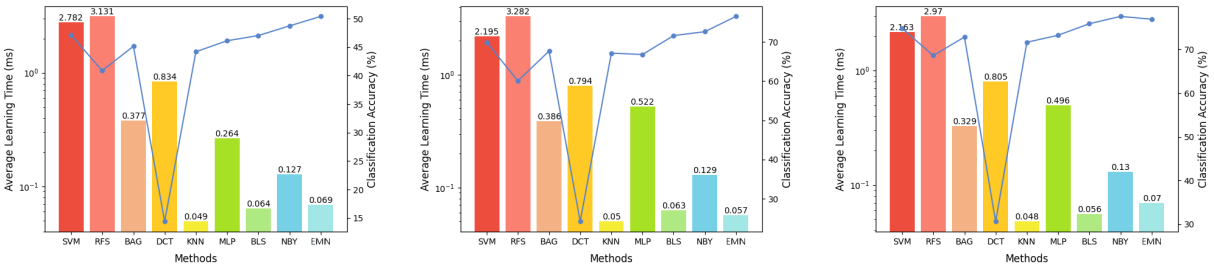

(a) $A \rightarrow C$ (b) $A \rightarrow P$ (c) $A \rightarrow R$

Figure 9. Accuracy versus the average domain adaptation time per instance on the Office-Home dataset dataset.

A.3. Accuracy in Different Epochs of Domain Adaptation

The accuracy of different models in different epochs of domain adaption is shown in Fig. 10, Fig. 11, Fig. 12, and Fig. 13.

A.4. Visualization

Fig. 14 depicts the memory units of randomly chosen neurons intuitively, which show diverse memory patterns on different neurons.

Based on the thresholding accumulation of transmitted signals, neurons can generate impulse signals like Fig. 15, which shares the similar intermittent property with the spiking activities in brains (Maass, 1997). On each round of propagation,

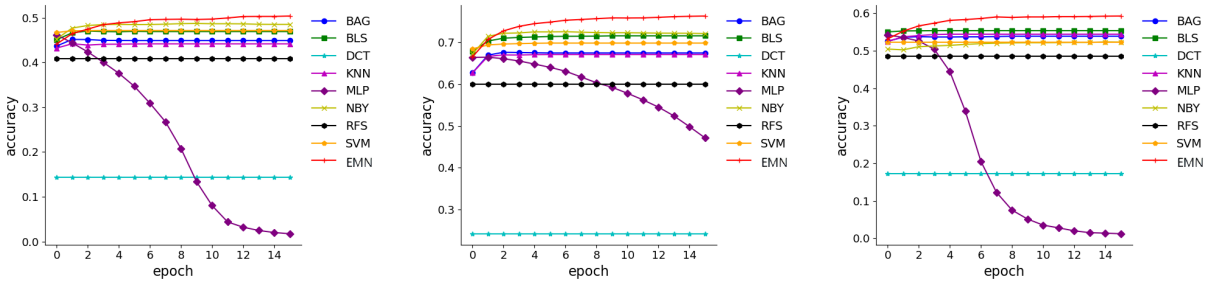

(a) $A \rightarrow C$ (b) $A \rightarrow P$ (c) $C \rightarrow A$

Figure 10. The accuracy in different epochs of domain adaptation on the Office-Home dataset.

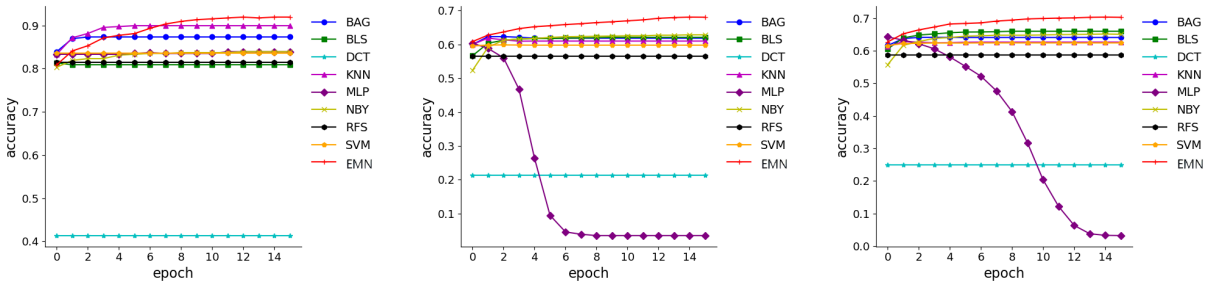

(a) $A \rightarrow D$ (b) $D \rightarrow A$ (c) $W \rightarrow A$

Figure 11. The accuracy in different epochs of domain adaptation on the Office-31 dataset.

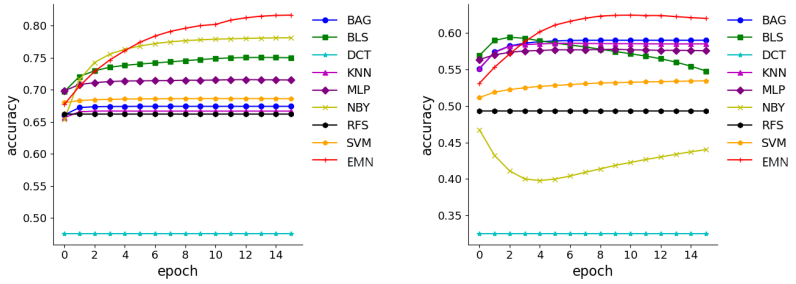

(a) $R \rightarrow S$ (b) $S \rightarrow R$

Figure 12. The accuracy in different epochs of domain adaptation on the VisDA-C dataset.

only a portion of nodes are activated in the network and the left accumulate the signals in their hidden states.

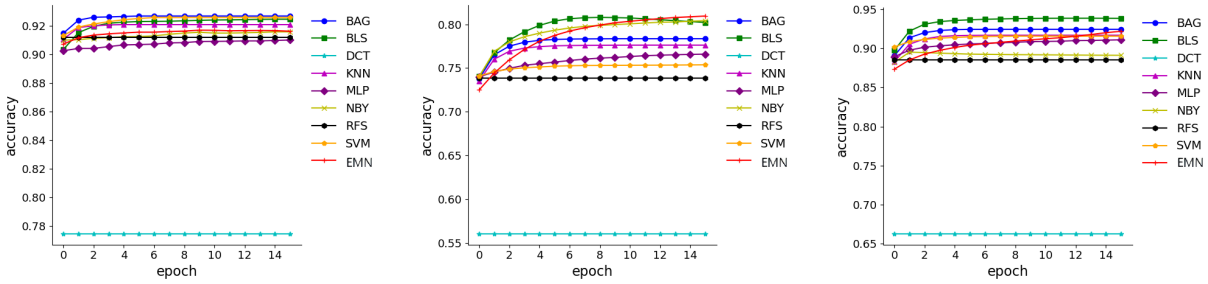

(a) $M \rightarrow U$ (b) $S \rightarrow M$ (c) $U \rightarrow M$

Figure 13. The accuracy in different epochs of domain adaptation on the Digits dataset.

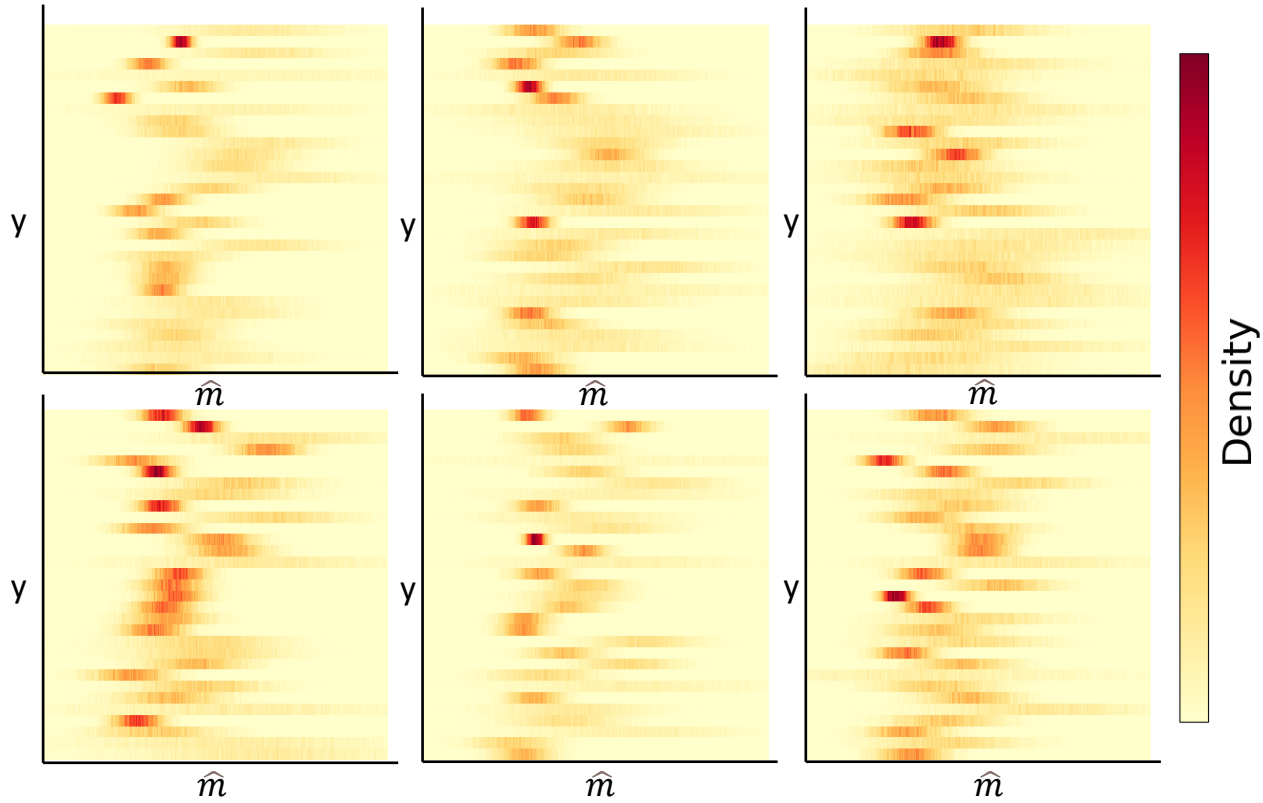

Figure 14. Visualization of the memories on six randomly chosen neurons after training on the Office-31 dataset

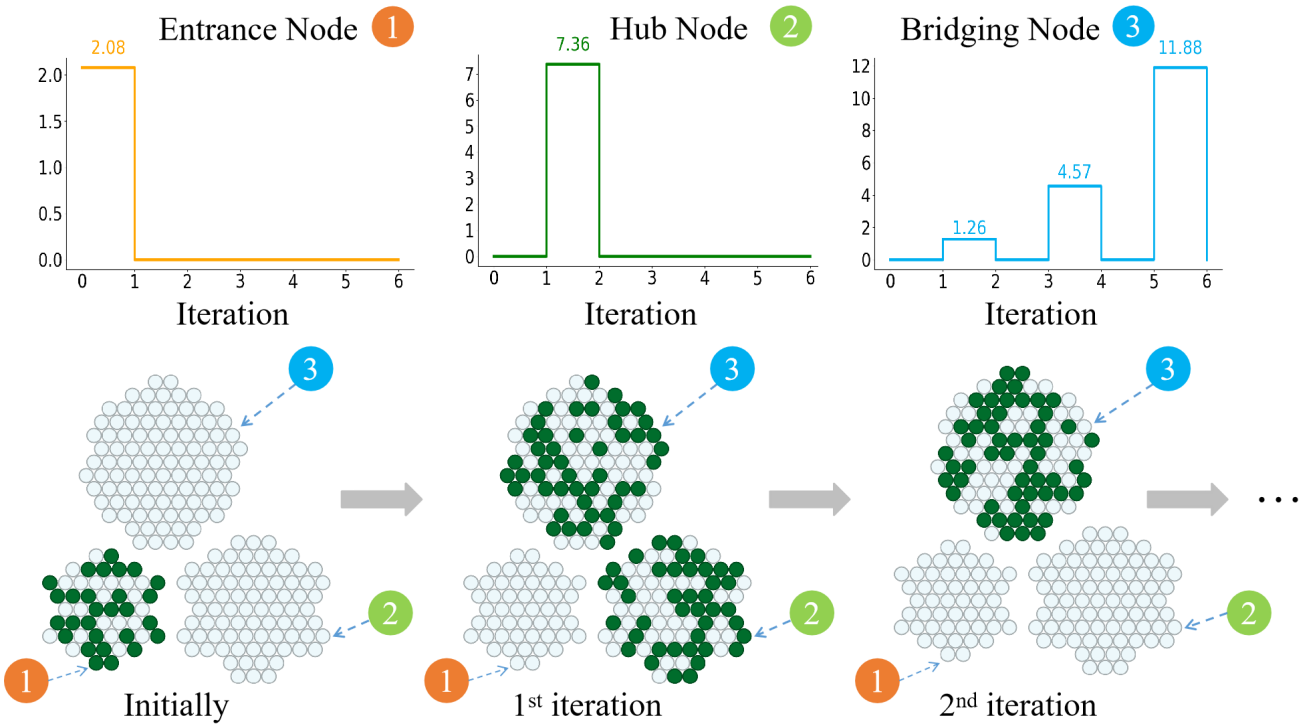

Figure 15. The change of the activation states and the output signals $o_{i,t}$ of the neurons in different iterations of signal propagation. For simplicity, we only show the nodes here while ignoring the connections. The green nodes indicate the activated ones with non-zero output.